

Achieving metrological precision limits through postselection

G. Bié Alves, A. Pimentel, M. Hor-Meyll, S. P. Walborn, L. Davidovich, and R. L. de Matos Filho

Instituto de Física, Universidade Federal do Rio de Janeiro, P.O. Box 68528, Rio de Janeiro, Rio de Janeiro 21941-972, Brazil

(Received 10 June 2016; published 6 January 2017)

Postselection strategies have been proposed with the aim of amplifying weak signals, which may help to overcome detection thresholds associated with technical noise in high-precision measurements. Here we use an optical setup to experimentally explore two different postselection protocols for the estimation of a small parameter: a weak-value amplification procedure and an alternative method that does not provide amplification but nonetheless is shown to be more robust for the sake of parameter estimation. Each technique leads approximately to the saturation of quantum limits for the estimation precision, expressed by the Cramér-Rao bound. For both situations, we show that parameter estimation is improved when the postselection statistics are considered together with the measurement device.

DOI: [10.1103/PhysRevA.95.012104](https://doi.org/10.1103/PhysRevA.95.012104)

I. INTRODUCTION

Reaching the ultimate precision limits in the estimation of parameters is an important challenge in science. Usually, this estimation is made by measuring the state of a probe that has undergone a parameter-dependent process. Postselection techniques, stemming from the pioneering work of Aharonov *et al.* [1,2], have been proposed with the aim of amplifying the signal obtained from the probe. In this formulation, the quantum system being analyzed gets coupled to a measuring apparatus (usually called a meter) through a unitary operation, which involves operators \hat{A} for the system \mathcal{A} and \hat{M} for the meter \mathcal{M} , and depends on the parameter g to be estimated. The goal is to estimate g by measuring the change of an observable of the meter after the joint unitary evolution, given that a specified state of \mathcal{A} was successfully postselected. For a small coupling constant g , the shift of the mean value of the relevant meter observable is modified by a prefactor, known as the weak-value $A_w = \langle \psi_f | \hat{A} | \psi_i \rangle / \langle \psi_f | \psi_i \rangle$, where $|\psi_i\rangle$ and $|\psi_f\rangle$ are the initial and the postselected states of \mathcal{A} , respectively. This quantity allows one to observe amplification effects provided the initial and the final state of the system are almost orthogonal, so long as the weak-value regime remains valid. The regime of validity of this result has been analyzed in several publications [3–5].

The possibility of amplifying a tiny displacement of the meter, weak-value amplification (WVA), has been envisaged as a valuable resource for the estimation of the coupling constant g , eventually circumventing technical thresholds that may hinder the evaluation of this parameter [6–9]. Weak-value amplification experiments have been performed with this metrological purpose [10–12], while claiming practical advantages. Moreover, alternative protocols have been proposed [13,14] to enhance the precision of the technique. However, there has been a long debate in the literature whether this postselection process can actually be beneficial for parameter estimation [6–9,15–19]. Indeed, the amplification of the signal comes at the cost of discarding most of the statistical data, due to the postselection procedure.

Here we experimentally investigate the estimation of a small deflection g of a mirror inside a Sagnac interferometer within the framework of quantum metrology. We employ two postselection protocols, which were shown [5] to lead to the

ultimate quantum limits for precision, for sufficiently small g . In the first one, related to the WVA approach, we explore the region of validity of WVA and show that, beyond this region, when the meter does not give useful information on g , estimation of this parameter can be obtained from the statistics of postselection [5]. We also experimentally demonstrate a postselection procedure that, even though not leading to WVA, may also reach the fundamental limits of precision, but with a much larger postselection probability. This implies that the number of events registered by measuring the meter is much larger than that in the WVA scheme, for the same amount of resources. This reflects in our experimental results, which clearly show that this second procedure leads to a more efficient determination of probabilities regarding the meter, in terms of frequencies of clicks in the measurement apparatus.

This paper is organized as follows. In Sec. II we present our experimental setup as well as the relevant metrological limits for parameter estimation. In Sec. III we introduce the methodology used to acquire information about g from both the meter and the postselection statistics. Our experimental results for two different postselection strategies are discussed in detail in Sec. IV. A summary is provided in Sec. V.

II. EXPERIMENTAL SETUP

The experimental setup is shown in Fig. 1. A red diode laser ($\lambda = 650$ nm) is sent through a single-mode optical fiber (SM Fiber) and decoupled by an objective lens, producing, in a good approximation, a collimated free-space Gaussian beam with a width $\Delta = 286$ μm . A 650 ± 13 nm bandpass filter removes unwanted light. The polarization degree of freedom corresponds to the *system*, while the transverse spatial degree of freedom of the beam stands for the *meter*. A polarizing beam splitter (PBS1) and a half waveplate (HWP1) are used to prepare a linear-polarization state $|\psi_i\rangle$. Accordingly, the system-meter input state for the interferometer is well described by

$$|\Psi_i\rangle \equiv |\psi_i\rangle \otimes |\phi_i\rangle = [\cos(\theta_i/2)|H\rangle + \sin(\theta_i/2)|V\rangle] \otimes |\phi_i\rangle, \quad (1)$$

where $|H\rangle$ and $|V\rangle$ represent the horizontal and vertical polarization states, respectively, and $|\phi_i\rangle$ stands for the

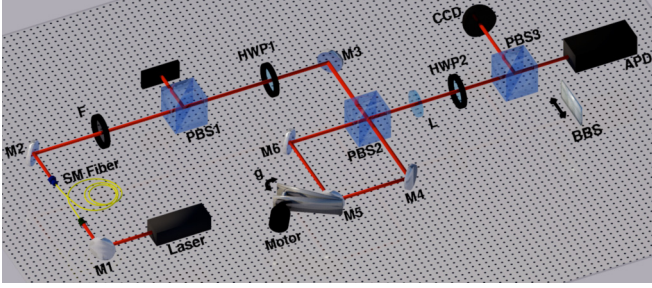


FIG. 1. Experimental setup. The goal is to estimate the deflection of a mirror, represented by g . See the text for a complete description of the experiment.

initial transverse spatial state. The Sagnac interferometer is composed of three mirrors (M4–M6) and a polarizing beam splitter (PBS2). The horizontal polarization component of the input beam propagates through the interferometer in the clockwise direction, while the vertical one circulates in the counterclockwise direction, recombining again at PBS2. A stepper motor controls the deflection angle of mirror M5. This results in transverse momentum shifts in opposite directions for the horizontal- and vertical-polarized components, respectively. Therefore, the overall effect of the interferometer on the input beam can be represented by the unitary operator

$$\hat{U} = e^{-ig\hat{\sigma}_3\hat{x}}, \quad (2)$$

where $\hat{\sigma}_3 = |H\rangle\langle H| - |V\rangle\langle V|$, \hat{x} represents the transverse position operator, and g is the shift in transverse momentum, which is much smaller than the wave number k_0 of the light beam. After the interferometer, a $f = 250$ mm lens (L) implements a Fourier transform of the transverse spatial field at mirror M5 onto the detection plane, defined by the detection aperture of a single-photon avalanche detector (APD). The polarization measurement setup consists of a half waveplate (HWP2) and a polarizing beam splitter (PBS3), which allows for postselecting any linear polarization state $|\psi_f\rangle$. A sliding beam-blocking stage (BBS) is used for the meter measurement after postselection. This system works like a quadrant detector. The detection aperture of the APD is 8 mm in diameter, much larger than the beam. By counting photons while blocking half of the detector, we can determine the center of the beam, as will be discussed below.

The Cramér-Rao inequality provides the lower bound on the uncertainty δg in the estimation of the parameter g : $\delta g \geq 1/\sqrt{\nu F(g)}$. Here ν is the number of repetitions of the measurement and $F(g)$ is the Fisher information, defined by $F(g) = \sum_j [1/P_j(g)] [dP_j(g)/dg]^2$, where $P_j(g)$ is the probability of obtaining experimental result j , given that the value of the parameter is g . The maximization of $F(g)$ over all possible measurements on the system yields the *quantum* Fisher information [20,21], which provides the ultimate precision bounds. For pure initial states and unitary evolutions, it is given by $\mathcal{F} = 4(\Delta\hat{H})^2 = 4(\langle\hat{H}^2\rangle - \langle\hat{H}\rangle^2)$, where \hat{H} is the generator of the unitary transformation and the averages are taken with respect to the initial quantum state. From Eq. (2), $\hat{H} = \sigma_3\hat{x}$, so, assuming that initially $\langle\hat{x}\rangle = 0$ (balanced-meter condition), one has $\mathcal{F} = 4\langle\hat{x}^2\rangle$, where the average is taken in the initial state $|\phi_i\rangle$ of the meter. Therefore,

the larger the variance of position in the initial state of the meter, the more information about the parameter is imprinted by the unitary evolution on the state of the system plus the meter.

Under postselection on a state $|\psi_f\rangle$ of the system, the Fisher information about g can be decomposed as [5,22] $F_{ps}(g) = p_f(g)F_m(g) + F_{p_f}(g)$, where $F_m(g)$ is the Fisher information associated with measurements on the state of the meter after postselection, $p_f(g)$ is the probability that the postselection succeeds, and

$$F_{p_f}(g) = \frac{1}{p_f(g)[1 - p_f(g)]} \left[\frac{dp_f(g)}{dg} \right]^2 \quad (3)$$

is the Fisher information on g corresponding to $p_f(g)$.

In [5] it was shown that, for sufficiently small g and for optimal measurement on the meter, postselection on either the state $|\psi_f\rangle = \hat{A}|\psi_i\rangle/\sqrt{\langle\hat{A}^2\rangle}$ or the state $|\psi_f\rangle = |\psi_i\rangle$ leads to a value of F_{ps} that coincides with the quantum Fisher information $\mathcal{F}(g)$, up to terms of $O(g^2)$. Therefore, under these conditions, this procedure yields optimal information on the parameter. These results, developed in [5], differ from the standard WVA approach in two important features: (i) the best postselection is *not* on a state of \mathcal{A} quasiorthogonal to the initial state and (ii) one should consider, in general, the statistics of postselection, in addition to the results stemming from measurements on the meter. The choice $|\psi_f\rangle = |\psi_i\rangle$ does not lead to WVA, but implies a probability of postselection much higher than the WVA procedure. We will show in this paper that this results in a more reliable determination of the probability distribution of the displacement of the meter, which is used for the estimation of g .

III. EXPERIMENTAL PROCEDURE

The experiment consists in applying a small misalignment g to mirror M5, sending light in the state $|\psi_i\rangle \otimes |\phi_i\rangle$ into the interferometer, recording the statistics of postselection events on the polarization state $|\psi_f\rangle$, and measuring the mean transverse momentum of the light beam, after successful postselection on $|\psi_f\rangle$. From the data one finally extracts an estimation for g , using a maximum-likelihood estimator. The postselection probability $p_f(g)$ is obtained by measuring, without the BBS, the photon counts N_f reaching the APD when the setup is adjusted for postselecting the state $|\psi_f\rangle$, as well as the photon counts N_f^\perp corresponding to the state orthogonal to $|\psi_f\rangle$. For a large number of counts, $p_f(g)$ is given by

$$p_f(g) = \frac{N_f(g)}{N_f(g) + N_f^\perp(g)}. \quad (4)$$

The corresponding theoretical model leads to (see the Appendix, Sec. 1)

$$p_f(g) = \frac{1}{2}(1 + v_0 \cos^2 \theta_i \pm v_{\pi/2} \sin^2 \theta_i e^{-2g^2 \Delta^2}), \quad (5)$$

where the + (−) sign corresponds to the postselection $|\psi_f\rangle = |\psi_i\rangle$ ($|\psi_f\rangle = \hat{\sigma}_3|\psi_i\rangle$), $v_{\pi/2}$ is the visibility of the interferometer, and v_0 is related to the extinction ratio of the polarization optics. We measured these visibilities in our experiment before the mirror angle is displaced ($g = 0$), by

preparing the polarization states $|\psi_i\rangle = |H\rangle$ and $|\psi_i\rangle = |+\rangle = (|H\rangle + |V\rangle)/\sqrt{2}$ and measuring photocounts N as a function of the HWP2 angle, after subtracting photocounts due to ambient noise. Visibility was determined using the usual formula $\nu = (N_{\max} - N_{\min})/(N_{\max} + N_{\min})$. For our alignment conditions, we obtained $\nu_{\pi/2} = 0.966$ and $\nu_0 = 0.998$; the latter was expected to be very close to unity, provided the high efficiency of the waveplates.

All of the information about g that is encoded in the meter state $|\phi_f\rangle$ can be retrieved via an optimal projective measurement. As described in [5], measurement of the observable $\hat{W} = \hat{k}$, conjugate to $\hat{M} = \hat{x}$, is optimal for both postselection procedures, as long as the meter state remains Gaussian after the postselection. In fact, in the region of validity of the WVA, the distribution of the eigenvalues of the observable \hat{k} in the final meter state remains Gaussian, with the same variance as in the initial state and shifted mean [2,5]. In this situation, measurement of the mean value $\langle\hat{k}\rangle$ is equivalent to measurement of \hat{k} . At the focal plane of the lens L, a shift in the mean transverse momentum $\langle\hat{k}\rangle$ of the beam at mirror M5 is converted into a displacement of the beam center, given by

$$d = f\langle\hat{k}\rangle/k_0, \quad (6)$$

where $k_0 = 2\pi/\lambda$, while the beam is resized to $\Delta_f = f/2k_0\Delta$. For this reason, in order to measure a shift in $\langle\hat{k}\rangle$, the beam center is measured with the BBS positioned at the focal plane of the lens L. Information about the beam displacement is then obtained via measurement of the number of photons reaching the two halves of the transverse plane during a given sampling time, which is equivalent to a split detector technique [23,24]. For a Gaussian beam with diameter Δ_f (at the focus), subjected to a displacement d , we have

$$\frac{|N_R - N_L|}{N_R + N_L} = \sqrt{\frac{2}{\pi}} \frac{d}{\Delta_f}, \quad (7)$$

where N_L (N_R) is the number of photons detected on the left (right) half plane. The corresponding theoretical model, taking into account the imperfect visibility, yields for the mean momentum deflection (see the Appendix, Sec. 2)

$$\langle\hat{k}\rangle = \frac{-g(\nu_0 + 1)\cos\theta_i}{1 + \nu_0\cos^2\theta_i \pm \nu_{\pi/2}\sin^2\theta_i e^{-2g^2\Delta^2}}. \quad (8)$$

To utilize this split detector technique, one has to calibrate the detector before the interferometer is misaligned ($g = 0$) to set the reference point. This is realized by matching the counts in the two halves of the detector (within statistical fluctuations of the photocounts) when the preselected and postselected states are $|+\rangle$ (for which $\theta_i = \pi/2$), once this postselection scheme is expected to have a null displacement according to Eq. (8) for any value of the coupling g . After displacing the mirror M5, we are able to measure the new values of the intensities N_L and N_R by sequentially inserting and removing the BBS at the same position for the each postselected state. However, the calibration was realized with a micrometer (10- μm precision, mounted on the BBS), which did not have the desired precision. We then added a constant to the theoretical displacement by simply replacing $d \mapsto d + d_0$, to account for any experimental error in the reference point, which best describes the data set. It is expected that this

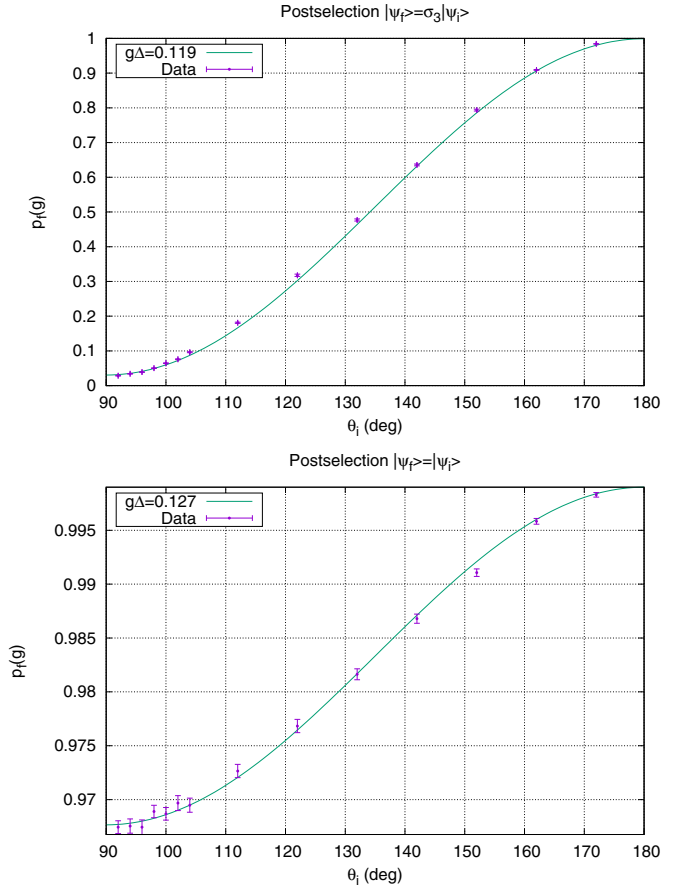


FIG. 2. Measured postselection probability as a function of the initial polarization state for strategies $|\psi_f\rangle = \hat{\sigma}_3|\psi_i\rangle$ (top) and $|\psi_f\rangle = |\psi_i\rangle$ (bottom).

constant d_0 should be very small compared to the beam size at the focus, which was confirmed by our data (see Fig. 3).

IV. EXPERIMENTAL RESULTS

We send on average $N \approx 10^5$ photons into the interferometer and determine $p_f(g)$ and $\langle\hat{k}\rangle$ as described above. From the measured data we obtain an estimate for g via a maximum-likelihood estimator (see the Appendix, Sec. 3). In order to access the precision of the estimation procedure and compare it with the theoretical bounds, we repeated this measurement process 100 times and used the variance of the resulting estimates of g as the uncertainty in our estimation procedure.

Figures 2 and 3 show the experimental results for the postselection measurements and meter shift. In all plots the curve joining the experimental data (dots) is a fit of the parameter $g\Delta$ for the given visibilities ν_0 and $\nu_{\pi/2}$ measured experimentally before the interaction is applied. The experimental data are in good agreement with the proposed theoretical model for the postselection probability, as given by Eq. (5), as well as for the mean beam displacement, as given by Eqs. (6) and (8), for both types of postselection strategies. It is worth noting in Fig. 3 that there is an amplification effect for the case $|\psi_f\rangle = \hat{\sigma}_3|\psi_i\rangle$, as seen from the graph. However, as

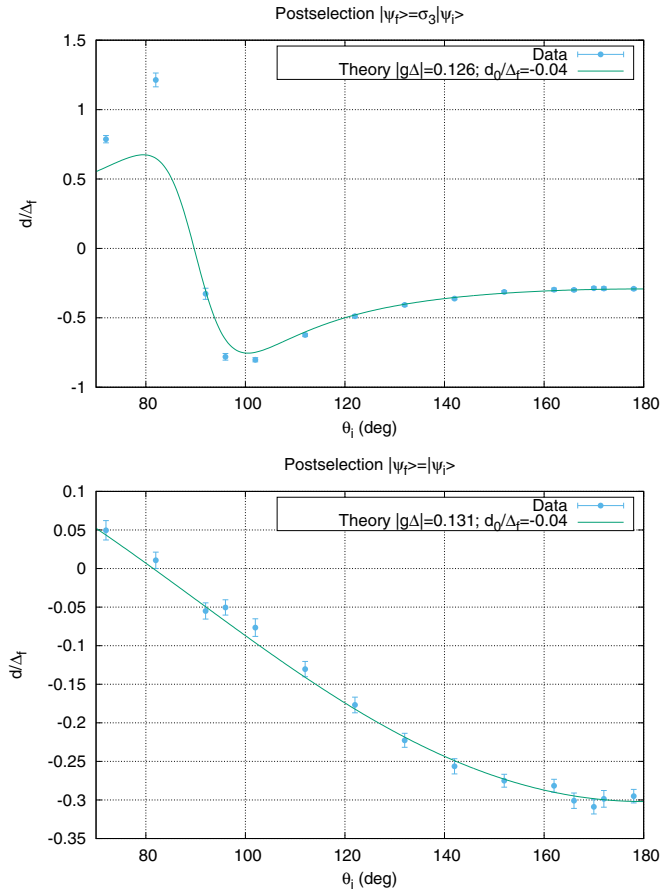


FIG. 3. Measured meter shift as a function of the initial polarization state for strategies $|\psi_f\rangle = \hat{\sigma}_3|\psi_i\rangle$ (top) and $|\psi_f\rangle = |\psi_i\rangle$ (bottom). Shown is the inferred shift of the Gaussian wave packet using the BBS technique for different initial polarization states in the Bloch sphere.

the amplification gets stronger, the wave function gets distorted and the BBS technique does not capture the correct shift (since it is meant to work for a Gaussian wave packet), as one can see from the points closer to the peaks. There is no amplification in the case $|\psi_f\rangle = |\psi_i\rangle$.

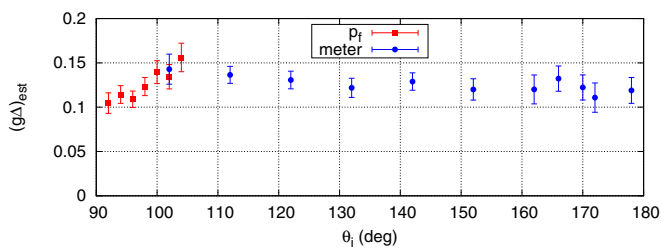


FIG. 4. Estimated value of $g\Delta$ from the experiment, for postselection in $|\psi_f\rangle = \hat{\sigma}_3|\psi_i\rangle$. Blue circles correspond to estimates from measurements on the meter, while red squares correspond to estimates obtained via the statistics of postselection events. Error bars represent $3\text{-}\sigma$ dispersion. Due to the mutually exclusive nature of the information obtained from meter and postselection statistics, there is no advantage in considering them together in the estimation of $g\Delta$.

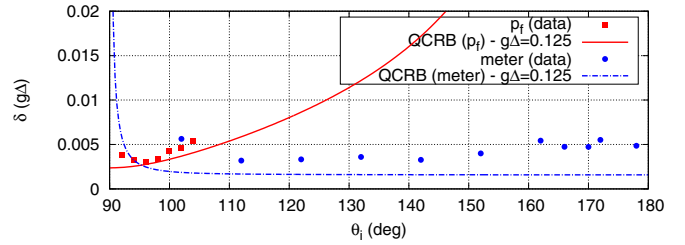


FIG. 5. Comparison between theoretical and experimental uncertainties for estimation of the dimensionless parameter $g\Delta$ as a function of the initial state $|\psi_i\rangle$, for the postselection $|\psi_f\rangle = \sigma_3|\psi_i\rangle$. The measured uncertainties are shown for estimation via the statistics of postselection events (red squares) and measurement on the meter state (blue circles). The red solid and blue dash-dotted lines show the corresponding quantum bounds, taking into account the imperfections in the interferometer.

Figure 4 shows the estimated values of the dimensionless parameter $g\Delta$ as a function of the angle θ_i that defines the initial state $|\psi_i\rangle$, for the postselection procedure related to the WVA, where $|\psi_f\rangle = \hat{\sigma}_3|\psi_i\rangle$. Notice that, in contrast to traditional WVA approaches, the postselection is not, in general, in a state quasiorthogonal to $|\psi_i\rangle$. As $|\psi_f\rangle$ approached orthogonality to $|\psi_i\rangle$, we could not provide reliable estimates for $g\Delta$ based on measurements on the meter alone. In our experiment this corresponds to the region $90^\circ \lesssim \theta_i \lesssim 100^\circ$, due to the value of $g\Delta$ used in the experiment. There are both fundamental and practical reasons for this. First, the wave packet of $|\phi_f\rangle$ begins to distort and lose its Gaussian shape. As a result, direct measurement of the mean value $\langle \hat{k} \rangle$ is no longer optimal and the split detector is unable to measure the displacement of the non-Gaussian beam correctly. Finally, the quantity of information about g encoded in the meter drops sharply to zero. However, in exactly this region where there is almost no information about the parameter g in the state of the meter and the WVA approach is no longer applicable, we have obtained excellent estimates of $g\Delta$ by considering only the postselection probability $p_f(g)$. Thus, by taking into account information from both the meter and the postselection statistics, we are able to provide consistent estimates of $g\Delta$ for all values of θ_i .

In Fig. 5 we compare the experimental uncertainties in the estimation of the dimensionless parameter $g\Delta$ with the corresponding quantum Cramér-Rao bounds (QCRBs), where we have taken into account the imperfect visibility of the interferometer. No other experimental imperfections are considered. This figure shows that our approach, based on the prevalence of the meter and the postselection statistics in different regions, leads to uncertainties very close to the theoretical bounds.

It is important to notice also that the mean number of photons used to estimate $\langle \hat{k} \rangle$ from the meter decreases steadily as θ_i decreases from 180° to 90° ($\langle \psi_f | \psi_i \rangle \rightarrow 0$). Since the maximum-likelihood estimator is only asymptotically consistent, the reduction in the number of photons used in the estimation of the parameter $g\Delta$ via measurement on $|\phi_f\rangle$ impairs the performance of the estimator, increasing its bias and uncertainty. This is a drawback of postselection procedures

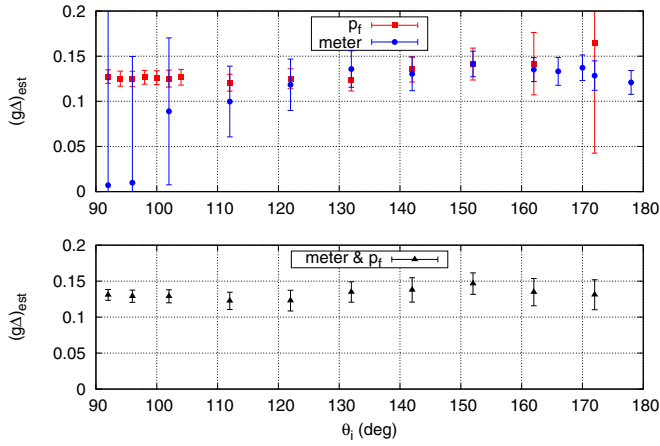


FIG. 6. Estimated value of $g\Delta$ from the experiment, for postselection in $|\psi_f\rangle = |\psi_i\rangle$. Blue circles correspond to estimates from measurements on the meter, red squares correspond to estimates obtained via the statistics of postselection events, and black triangles correspond to estimates using information of both the meter and the statistics of postselection events. Error bars represent $3\text{-}\sigma$ dispersion.

related to WVA when compared to other strategies, if the total resources used in the experiment (photon number in our case) are kept constant.

We consider now the second postselection strategy, which relies on postselection onto $|\psi_f\rangle = |\psi_i\rangle$. Figure 6 shows the estimated values of $g\Delta$ as a function of the initial state $|\psi_i\rangle$ for this case. Contrary to the first case, here information about the parameter g is distributed among the meter and the postselection statistics for almost the whole range of θ_i values [5]. As a result, the best estimation of the parameter $g\Delta$ is provided by using data from both the meter and the statistics of postselection events. Information about g encoded in the statistics of postselection events begins to decrease for $\theta_i \approx 160^\circ$ and is zero for $\theta = 180^\circ$. This explains the increase in the error bars of the corresponding estimates for this range of values of θ_i . On the other hand, information about g encoded in the meter dwindles when θ_i decreases from 120° to 90° , but never goes to zero. The degradation of the corresponding estimates in the region between 110° and 90° is due to the fact that measuring $\langle \hat{k} \rangle$ is no longer optimal and in fact the information about g extractable via $\langle \hat{k} \rangle$ does go to zero as the value of θ_i approaches 90° . This behavior is clearly displayed in Fig. 7, which compares the experimental uncertainties in the estimation of the dimensionless parameter $g\Delta$. As before, the QCRB takes into account the slightly reduced visibility of the interferometer and no other experimental imperfection. Figure 7 also shows that the experimental uncertainty in the estimates produced from information of both the meter and the statistics of postselection events is very close to the theoretical quantum bounds for all values of θ_i .

It is important to notice that, contrary to the WVA postselection procedure, the probability of successful projection onto $|\psi_f\rangle = |\psi_i\rangle$ is close to unity for the whole range of values θ_i . Thus, the mean number of photons used to estimate $\langle \hat{k} \rangle$ from the meter remains very close to the total number of photons injected into the interferometer and does not lead to the degradation of the performance of the maximum-likelihood

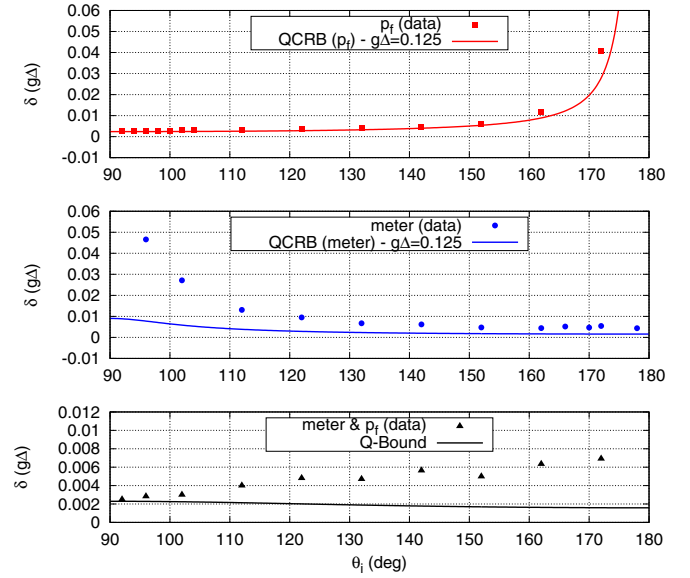


FIG. 7. Comparison between theoretical and experimental uncertainties for estimation of the dimensionless parameter $g\Delta$ as a function of the initial-state parameter θ_i , for the postselection $|\psi_f\rangle = |\psi_i\rangle$. The measured uncertainties (red squares, blue circles, and black triangles) are shown for estimation via the statistics of postselection events (top), measurement on the meter state (middle), and using information of both the meter and the statistics of postselection events (bottom). The lines show the corresponding quantum bounds on precision (see the text). The scale of the bottom figure is highly amplified.

estimator, as was the case for the WVA-related strategy. Furthermore, the Fisher information corresponding to $p_f(g)$ is now relevant over a wider range of initial states, as compared to the previous postselection scheme, which is yet another advantage of the present procedure, since measuring $p_f(g)$ is simple to implement and is always optimal, independently of the initial state. This is in stark contrast to optimal measurements on the meter, which depend on the initial state and are therefore more challenging to implement. These two facts lead to the consistency of the estimates for any initial state $|\psi_i\rangle$, as shown in Fig. 6, which result in a highly effective and robust metrological protocol that can, in principle, reach the ultimate precision bounds on parameter estimation.

V. CONCLUSION

We have experimentally investigated two postselection-based measurement procedures from a quantum metrology point of view. One of these is a postselection procedure that presents considerable advantages over the weak-value amplification scheme. The first method considered in this paper, related to the WVA procedure, fails to provide a reasonable estimation of the parameter (tilt of a mirror in the interferometer, described by g) from the state of the meter alone when the postselection is around the region of highest amplification. In this same region, the non-Gaussian profile of the wave packet describing the meter makes it difficult to implement an optimal measurement on it. Furthermore, the reduction in the number of probe photons, due

to the postselection on a nearly orthogonal state, impairs the performance of the corresponding estimator. We show that accurate estimation of g can be performed in this case when the statistics of the postselection of the system are taken into account. In the second method, there is almost no reduction in detection events due to postselection, since the corresponding probability remains close to one for all initial states. This leads to better performance of the meter estimator. In addition, information on g is now distributed between the meter and the postselection statistics over a wider range of initial states, allowing one to benefit from the information encoded in the postselection statistics, which is simple to obtain experimentally from a measurement procedure that is always optimal, regardless of the initial state. This method leads to uncertainties in the estimation of g that are closer to the quantum Cramér-Rao bound, particularly in the region where the information from the postselection statistics is dominant.

Our experiment serves as a proof-of-principle demonstration that postselection protocols can be metrologically efficient, as long as the information encoded in the postselection statistics is also taken into account. It also throws light on the subtle connection between postselection procedures and quantum metrology, offering a viable and easy-to-implement procedure that can be easily generalized to other parameter estimation tasks.

ACKNOWLEDGMENTS

This research was supported by the Brazilian agencies FAPERJ, CNPq, CAPES, and the National Institute of Science and Technology for Quantum Information.

APPENDIX: ADAPTING THE THEORETICAL MODEL TO THE EXPERIMENTAL CONDITIONS

1. Postselection probability

As described in the main text, the expected interaction implemented between the system and the meter by the Sagnac interferometer would correspond to a unitary operator $\hat{U}_g = e^{-ig\hat{\sigma}_3\hat{x}}$, as in Eq. (2). This leads to a probability of postselection given by

$$p_f(g) = |\langle \psi_f | \hat{U} | \psi_i \rangle \langle \phi_i | \rangle|^2 = \frac{1}{2}(1 + \cos^2 \theta \pm e^{-2g^2 \Delta^2} \sin^2 \theta), \quad (\text{A1})$$

where the $+$ ($-$) sign corresponds to the postselected state $|\psi_f\rangle = |\psi_i\rangle$ ($|\psi_f\rangle = \hat{\sigma}_3 |\psi_i\rangle$). However, one can easily see that, before the interaction takes place ($g = 0$), the postselection probability onto the same initial state ($|\psi_f\rangle = |\psi_i\rangle$) is 1 irrespective of the initial state on the Bloch sphere. This implies that the visibility of the interferometer should be 100%, whatever the initial state is, which does not correspond to the real experimental conditions, where tiny unwanted misalignment of the interferometer may affect the quality of the interference.

To account for a small relative misalignment in the y direction (perpendicular to x , in the transverse plane), it is enough to consider the same interaction, but now being implemented by $\hat{U}_w = e^{-iw\hat{\sigma}_3\hat{y}}$. Thus, the complete evolution

would be described by

$$\hat{U}_w \hat{U}_g |\psi_i\rangle |\phi_i\rangle |\varphi_i\rangle, \quad (\text{A2})$$

where it is supposed that the spacial state is a product state between the directions x and y , represented by $|\phi_i\rangle$ and $|\varphi_i\rangle$.

The probability of postselection is then given by

$$\begin{aligned} p_f(g) &= \text{Tr}(\hat{P}_f \hat{U}_w \hat{U}_g |\psi_i\rangle \langle \psi_i| \otimes |\phi_i\rangle \langle \phi_i| \otimes |\varphi_i\rangle \langle \varphi_i| \hat{U}_w^\dagger \hat{U}_g^\dagger) \\ &= \text{Tr}_x[\hat{U}_g |\psi_i\rangle \langle \psi_i| \otimes |\phi_i\rangle \langle \phi_i| \otimes \hat{U}_g^\dagger \text{Tr}_y(|\varphi_i\rangle \langle \varphi_i| \hat{U}_w^\dagger \hat{P}_f \hat{U}_w)], \end{aligned} \quad (\text{A3})$$

where $\hat{P}_f = |\psi_f\rangle \langle \psi_f|$. However, we have that

$$\begin{aligned} \text{Tr}_y(|\varphi_i\rangle \langle \varphi_i| \hat{U}_w^\dagger \hat{P}_f \hat{U}_w) &= \langle \varphi_i | \hat{U}_w^\dagger \hat{P}_f \hat{U}_w | \varphi_i \rangle \\ &= \hat{P}_f \left[\int dy |\varphi(y)|^2 \cos^2(wy) \right] \\ &\quad + i[\hat{P}_f, \hat{\sigma}_3] \left[\int dy |\varphi(y)|^2 \sin(wy) \cos(wy) \right] \\ &\quad + \hat{\sigma}_3 \hat{P}_f \hat{\sigma}_3 \left[\int dy |\varphi(y)|^2 \sin^2(wy) \right] \\ &= (1 - p/2) \hat{P}_f + p/2 \hat{\sigma}_3 \hat{P}_f \hat{\sigma}_3, \end{aligned} \quad (\text{A4})$$

where $p/2 \equiv \int dy |\varphi(y)|^2 \sin^2(wy)$, since the wave function is Gaussian and the second term in Eq. (A4) vanishes. This implies that the evolution under the interaction \hat{U}_w leads to a *dephasing channel* when monitoring only the x direction:

$$\begin{aligned} p_f(g) &= \text{Tr}_x \sum_\mu (\hat{P}_f \hat{K}_\mu \hat{U}_g |\psi_i\rangle \langle \psi_i| \otimes |\phi_i\rangle \langle \phi_i| \otimes \hat{U}_g^\dagger \hat{K}_\mu^\dagger) \\ &\equiv \text{Tr}_x[\hat{P}_f \hat{\rho}'_{S,M}(g)], \end{aligned} \quad (\text{A5})$$

with $\hat{K}_1 = \sqrt{1 - p/2} \hat{1}$, $\hat{K}_2 = \sqrt{p/2} \hat{\sigma}_3$ (the Kraus operators), and $\hat{\rho}'_{S,M}(g) = \sum_\mu K_\mu \hat{U}_g |\psi_i\rangle \langle \psi_i| \otimes |\phi_i\rangle \langle \phi_i| \otimes \hat{U}_g^\dagger K_\mu^\dagger$.

Besides this effect, it is assumed in the theoretical model that the polarization state $|\phi_i\rangle$ is prepared with 100% efficiency. To account for partial coherence in the preparation of the system state, we add an orthogonal component in the density matrix of the original state:

$$\hat{\rho}_S^i = (1 - \epsilon) |\psi_i\rangle \langle \psi_i| + \epsilon |\psi_i^\perp\rangle \langle \psi_i^\perp|, \quad (\text{A6})$$

where ϵ is expected to be very small. Together with the dephasing channel, this leads to an evolution described by

$$\begin{aligned} \hat{\rho}_{S,M}^i &= \hat{\rho}_S^i \otimes |\phi_i\rangle \langle \phi_i| \mapsto \hat{\rho}'_{S,M}(g) \\ &= \sum_\mu \hat{K}_\mu \hat{U}_g (\hat{\rho}_S^i \otimes |\phi_i\rangle \langle \phi_i|) \hat{U}_g^\dagger \hat{K}_\mu^\dagger. \end{aligned} \quad (\text{A7})$$

After some straightforward calculation, the probability of postselection is given by

$$\begin{aligned} p_f(g) &= \sum_\mu \text{Tr}[\hat{P}_f \hat{K}_\mu \hat{U}_g (\hat{\rho}_S^i \otimes |\phi_i\rangle \langle \phi_i|) \hat{U}_g^\dagger \hat{K}_\mu^\dagger] \\ &= \frac{1}{2} [1 + (1 - 2\epsilon) \cos^2(\theta_i) \\ &\quad \pm (1 - 2\epsilon)(1 - p) \sin^2(\theta_i) e^{-2g^2 \Delta^2}], \end{aligned} \quad (\text{A8})$$

where the sign $+$ ($-$) corresponds to a postselection onto $|\psi_f\rangle = |\psi_i\rangle$ ($|\psi_f\rangle = \hat{\sigma}_3|\psi_i\rangle$). Defining the visibility for a given prepared initial state $|\psi_i\rangle$, before the interaction takes place, as

$$v_\theta = \frac{N_f(\theta) - N_f^\perp(\theta)}{N_f(\theta) + N_f^\perp(\theta)} = 2p_f(0)|_\theta - 1, \quad (\text{A9})$$

we can readily interpret the parameters ϵ and p in terms of interference visibility analyzed in different polarization bases (characterized by θ) such that the expression for the probability can be rewritten as

$$p_f(g) = \frac{1}{2}[1 + v_0 \cos^2(\theta_i) \pm v_{\pi/2} \sin^2(\theta_i) e^{-2g^2\Delta^2}]. \quad (\text{A10})$$

2. Meter analysis

Since our purpose is to measure the mean momentum shift in the transverse plane after the postselection (as long as the meter state remains Gaussian), we require expressions for the theoretical expected value of the operator \hat{k} , where $[\hat{x}, \hat{k}] = i$. Taking into account the decoherence channels presented in the preceding section, the meter state after the postselection is given by

$$\hat{\rho}_f''(g) = \frac{\sum_\mu \text{Tr}_S(\hat{P}_f \hat{K}_\mu \hat{U}_g \hat{\rho}_S^i \otimes |\phi_i\rangle\langle\phi_i| \hat{U}_g^\dagger \hat{K}_\mu^\dagger)}{p_f(g)}, \quad (\text{A11})$$

where $\text{Tr}_S(\cdot)$ is the trace over the system (polarization) space. The measurement of \hat{k} is then given by

$$\begin{aligned} \langle\hat{k}\rangle &= \text{Tr}_M[\hat{\rho}_f''(g)\hat{k}] \\ &= \frac{\sum_\mu \text{Tr}(\hat{k} \hat{P}_f \hat{K}_\mu \hat{U}_g \hat{\rho}_S^i \otimes |\phi_i\rangle\langle\phi_i| \hat{U}_g^\dagger \hat{K}_\mu^\dagger)}{p_f(g)}. \end{aligned} \quad (\text{A12})$$

After some straightforward calculation, we have

$$\langle\hat{k}\rangle = \frac{-g(v_0 + 1) \cos \theta_i}{1 + v_0 \cos^2 \theta_i \pm v_{\pi/2} \sin^2 \theta_i e^{-2g^2\Delta^2}}, \quad (\text{A13})$$

where the sign $+$ ($-$) corresponds to $|\psi_f\rangle = |\psi_i\rangle$ ($|\psi_f\rangle = \hat{\sigma}_3|\psi_i\rangle$).

3. Maximum-likelihood estimation

Here we describe how we provide estimates for the desired parameter g for each experimental measurement outcome. The maximum-likelihood estimation procedure consists of finding the value of the coupling g that best matches a given experimental result in terms of the probability of occurrence. Thus, the *estimator* for g is found to be the one that maximizes the theoretical probability associated with a certain measured outcome. For the case of estimation based solely on the postselection probability $p_f(g)$, this procedure leads to solving Eq. (4) for g . Analogously, for the estimation based on the meter measurements, the equation to solve is given by Eq. (7), with the aid of Eq. (8). However, for the estimation based on both results, the outcome is defined by the set of numbers $\{N_R, N_L, N_f^\perp\}$, where $N_R + N_L = N_f$. The likelihood probability is then given by

$$\mathcal{L} = P_R(g)^{N_R} P_L(g)^{N_L} [1 - p_f(g)]^{N_f^\perp}, \quad (\text{A14})$$

where $P_L(g)$ and $P_R(g)$ are the theoretical probabilities of the meter to be detected at the left and right halves of the detector, respectively. The estimator g_{est} is then found by solving

$$\left. \frac{\partial \ln \mathcal{L}}{\partial g} \right|_{g_{\text{est}}} = 0. \quad (\text{A15})$$

For the case of postselection $|\psi_f\rangle = |\psi_i\rangle$, the meter remains approximately Gaussian and the probabilities $P_{L,R}(g)$ can be calculated as

$$P_R(g) = p_f(g) - P_L(g) \approx \left[\frac{1}{2} + \frac{d}{\sqrt{2\pi}\Delta_f} \right] p_f(g), \quad (\text{A16})$$

where $d = f\langle\hat{k}\rangle/k_0$. Using Eqs. (A14), (A16), (A13), and (A10), one can finally solve Eq. (A15) by numerical methods, once there is no analytical solution.

-
- [1] Y. Aharonov, P. G. Bergmann, and J. L. Lebowitz, *Phys. Rev.* **134**, B1410 (1964).
[2] Y. Aharonov, D. Z. Albert, and L. Vaidman, *Phys. Rev. Lett.* **60**, 1351 (1988).
[3] I. M. Duck, P. M. Stevenson, and E. C. G. Sudarshan, *Phys. Rev. D* **40**, 2112 (1989).
[4] A. G. Kofman, S. Ashhab, and F. Nori, *Phys. Rep.* **520**, 43 (2012).
[5] G. B. Alves, B. M. Escher, R. L. de Matos Filho, N. Zagury, and L. Davidovich, *Phys. Rev. A* **91**, 062107 (2015).
[6] Y. Kedem, *Phys. Rev. A* **85**, 060102 (2012).
[7] A. Feizpour, X. Xing, and A. M. Steinberg, *Phys. Rev. Lett.* **107**, 133603 (2011).
[8] A. N. Jordan, J. Martínez-Rincón, and J. C. Howell, *Phys. Rev. X* **4**, 011031 (2014).
[9] N. Brunner and C. Simon, *Phys. Rev. Lett.* **105**, 010405 (2010).
[10] D. J. Starling, P. B. Dixon, A. N. Jordan, and J. C. Howell, *Phys. Rev. A* **80**, 041803 (2009).
[11] G. I. Viza, J. Martínez-Rincón, G. A. Howland, H. Frostig, I. Shomroni, B. Dayan, and J. C. Howell, *Opt. Lett.* **38**, 2949 (2013).
[12] G. I. Viza, J. Martínez-Rincón, G. B. Alves, A. N. Jordan, and J. C. Howell, *Phys. Rev. A* **92**, 032127 (2015).
[13] J. Dressel, K. Lyons, A. N. Jordan, T. M. Graham, and P. G. Kwiat, *Phys. Rev. A* **88**, 023821 (2013).
[14] S. Pang, J. Dressel, and T. A. Brun, *Phys. Rev. Lett.* **113**, 030401 (2014).
[15] G. C. Knee, G. A. D. Briggs, S. C. Benjamin, and E. M. Gauger, *Phys. Rev. A* **87**, 012115 (2013).
[16] S. Tanaka and N. Yamamoto, *Phys. Rev. A* **88**, 042116 (2013).
[17] C. Ferrie and J. Combes, *Phys. Rev. Lett.* **112**, 040406 (2014).
[18] J. Combes, C. Ferrie, Z. Jiang, and C. M. Caves, *Phys. Rev. A* **89**, 052117 (2014).

- [19] G. C. Knee, J. Combes, C. Ferrie, and E. M. Gauger, [Quantum Measurements and Quantum Metrology](#) **3**, 32 (2016).
- [20] S. L. Braunstein and C. M. Caves, [Phys. Rev. Lett.](#) **72**, 3439 (1994).
- [21] C. W. Helstrom, *Quantum Detection and Estimation Theory* (Academic, New York, 1976).
- [22] L. Zhang, A. Datta, and I. A. Walmsley, [Phys. Rev. Lett.](#) **114**, 210801 (2015).
- [23] C. A. J. Putman, B. G. D. Grooth, N. F. V. Hulst, and J. Greve, [J. Appl. Phys.](#) **72**, 6 (1992).
- [24] S. Barnett, C. Fabre, and A. Maitre, [Eur. Phys. J. D](#) **22**, 513 (2003).